Microstructure and tensile properties of Ti6Al4V/AM60B magnesium matrix composite

Ye, Haizhi; Liu, Xing Yang

Publisher's version / Version de l'éditeur:
https://doi.org/10.1016/j.jallcom.2005.04.175
Journal of Alloys and Compounds, 402, 1-2, pp. 162-169, 2005-07-14

Microstructure and tensile properties of Ti6Al4V/AM60B magnesium matrix composite

H. Z. Ye, X. Y. Liu*

Integrated Manufacturing Technologies Institute, National Research Council of Canada

London, ON, Canada N6G 4X8

*. Corresponding author: Tel: 1-519-430-7042, Fax: 1-519-430-7064, Email: xingyang.liu@nrc.gc.ca.

Abstract

The high specific strength of magnesium and its alloys/composites makes it an attractive material for aerospace and automotive industrial applications. However, magnesium alloys have low strength at high temperatures. Developing magnesium matrix composites is a promising approach to increase the mechanical properties of magnesium alloys at high temperatures. In the research reported in this paper, Ti6Al4V particulate-reinforced magnesium matrix composite Ti6Al4V/AM60B was fabricated by casting and hot isostatic pressing processes. The SEM/EDS and XRD microstructure examination reveals that a significant amount of Mn_5Al_8 intermetallic particles segregated at the Ti6Al4V/AM60B matrix interface. Within the Ti6Al4V content (up to 5vol.%) studied, the addition of Ti6Al4V particles was found to have no beneficial effect on the room temperature strength of the composite material, however, the ductility was reduced. The interface segregation of Mn_5Al_8 intermetallic particles is believed to be the cause.

Keywords: Metal matrix composite (A), Intermetallics (A), Casting (B), Segregation, Tensile properties

1. Introduction

Magnesium alloys have been attracting an increased interest for applications in the aerospace and automotive industry in recent years due to their lightweight and high specific strength. However, compared to other metallic structural materials, magnesium alloys have a relatively low absolute strength, especially at elevated temperatures. The need for high-performance and lightweight materials has led to extensive R&D efforts in the development of magnesium matrix composites. Conventionally, lightweight metals such as Mg and Al are reinforced with hard ceramic particles, whiskers or fibers. In such cases, the improvement in strength is normally at a cost of significantly reduced ductility and toughness. In comparison with ceramic reinforcements, metallic solids generally have a much better wettability with liquid metals [1], greater ductility, and higher mechanical and thermal compatibility with the metallic matrix, and can be potentially employed as a reinforcement component in metal matrix composites. Recent studies have explored the effect of some metallic reinforcements such as Ni [2], Cu [3], and Ti [4] particulates in a magnesium matrix. It was reported that the addition of these metallic particles into the magnesium matrix has resulted in better mechanical properties than those of the same matrix material with ceramic reinforcements [2-4].

The relatively low density of Ti (4.5 g/cm^3 [5]) makes it an attractive choice as a metallic reinforcement for magnesium materials. A recent study reported that the yield strength of

pure magnesium was increased from 100 MPa to 163 MPa and elongation from 7.7% to 11.1% by adding 2vol.% of elemental Ti particulates [4]. Ti6Al4V alloy has a density of 4.42 g/cm^3 [5] with a much greater strength than pure Ti. The yield strength and ultimate tensile strength of pure Ti are around 200 MPa and 350 MPa respectively. In comparison, those for Ti6Al4V are around 800 MPa and 900 MPa respectively [5]. With the expectation that Ti6Al4V is likely to produce a greater reinforcing effect than pure Ti in a magnesium matrix, the effect of Ti6Al4V particle addition into an AM60B magnesium alloy was examined in this study. This paper reports the microstructure and mechanical properties of the magnesium composite with Ti6Al4V particle reinforcements.

2. Experimental procedures

2.1. Material preparation:

An AM60B magnesium alloy was used as the matrix of the materials and its composition is shown in Table 1. Ti6Al4V powders with an average particle size of 45 μm and concentrations of 1%, 2% and 5% in volume, respectively, were added into the magnesium alloy during melting. The melting was conducted in a vacuum induction furnace, as schematically illustrated in Fig. 1. Before melting, the Ti6Al4V powders were placed with AM60B magnesium alloy in alternating layers to help their distribution in the melt. After the AM60B alloy was melted, the steel tubing for Ar gas and thermocouple was lowered into the melt, followed by bubbling Ar gas (industrial purity) into the melt at a pressure of 207 kPa for 5 minute at 700°C to further assist in distributing Ti6Al4V particles uniformly. The molten alloy was then poured into a steel crucible and solidified into an ingot. The cast ingots were subsequently consolidated by a hot isostatic pressing

(HIP) process to reduce the porosity. The HIP process was performed in Ar gas at 515°C and 103 MPa for 2 hours. An AM60B magnesium alloy without Ti6Al4V addition was also prepared under the same procedures and used as a reference.

After the casting and HIP process of the composite material, Ti6Al4V particles were extracted from the sample in an ethanol solution containing 10vol.% acetic acid to examine the possible changes occurring to the Ti6Al4V particles during the processing.

2.2. Material characterizations:

The microstructure of the samples was characterized using a Hitachi S-3500 scanning electron microscope (SEM) with an energy dispersive spectrometer (EDS) attachment. The structure of the extracted particles was analyzed with a Rigaku XRD diffractometer using Co-Kα radiation.

Flat specimens cut from the ingots after HIP process were used for tensile tests. The specimens had a total length of 100mm and a gauge length of 25 mm. The width and thickness of the gauge length section were 6mm and 3 mm, respectively. Tensile tests were carried out at room temperature, using an INSTRON 8516 machine at a crosshead speed of 10 mm/min. The tensile data reported in this study are an average of 5 measurements.

3. Results and discussion

3.1. Microstructure of Ti6Al4V/AM60B composite

SEM microstructures of the Ti6Al4V/AM60B composite with 5% of Ti6Al4V in volume before and after HIP are shown in Fig. 2. Two kinds of particles with different sizes and shapes were clearly observed in the magnesium matrix. The large particles were irregular in shape and about 20-100 μm in size, (labeled as *A* in Fig. 2), while the small particles were mostly equi-axed in shape and up to a few microns in size (labeled as *B* in Fig. 2). The compositions of these particles, along with that of the matrix, analyzed by SEM/EDS, are listed in Table 2. The elements in the matrix were primarily Mg and Al, as expected. In addition, a small amount of O was also detected. The compositions of the *A* type large particles indicated that they were Ti6Al4V. The *B* type fine particles contained mainly Al, Mn, and Mg. Because the *B* type particles were very small, mostly 2-3 μm in diameter, and EDS analysis usually excites an area size in the order of approximately 5 μm at the working condition [6], it is not clear whether, the Mg detected from the *B* type small particles came from the matrix or from the particle itself. Based on EDS analysis, the fine *B* type particles were either Mn-Al or Mn-Mg-Al intermetallic compounds such as $Al_{10}(MnMg)_3$ [7].

SEM microstructure examination of the whole ingot revealed that Ti6Al4V particles had a reasonably uniform distribution in the matrix, in spite of the difference in the densities of Ti6Al4V (4.42g/cm^3 [5]) and AM60B (1.80g/cm^3 [8]). The uniform distribution of Ti6Al4V particles can be attributed to good wettability between Ti6Al4V particles and AM60B melt, the alternating layer setup of the Ti6Al4V particles and AM60B alloy in the melting crucible, and the agitation of the melt by Ar gas during the melting.

In the as-cast samples, some pores were present in the matrix and also at the interface between the Ti6Al4V particles and matrix, (labeled as *C* in Fig. 2a and 2b). However, after HIP, these pores were not observed either in the matrix or at the Ti6Al4V/matrix interfaces, indicating that HIP process has significantly increased the density of the material. The relatively uniform distribution of Ti6Al4V particles within the ingot and removal of porosity in the samples after HIP process shows that porosity-free Ti6Al4V/AM60B composites with uniform reinforcement distribution can be achieved by combining Ar gas agitation during melting with subsequent HIP treatment of the ingot.

An important microstructural feature of the Ti6Al4V/AM60B composite is the segregation of the fine *B* type particles on the Ti6Al4V and AM60B matrix interface. Prior to HIP, segregation of these particles was observed on almost all the Ti6Al4V particles, as shown in Fig. 2b. However, after HIP, the segregation of these fine *B* type particles was observed less frequently on the Ti6Al4V and AM60B matrix interface, as shown in Fig. 2d. The results of detailed EDS analysis of the Ti6Al4V/Mg interfaces in the samples, before and after HIP respectively, are illustrated in Figs. 3-6.

Fig. 3 shows EDS line spectra across a Ti6Al4V particle and a matrix/particle interface in the Ti6Al4V/AM60B composite prior to HIP. Mg was detected only in the matrix. Ti and V were found only in Ti6Al4V particles. Al was relatively evenly distributed in both the matrix and Ti6Al4V particles, but with a clear enrichment at the matrix/particle interface. Mn also showed a clear enrichment at the matrix/particle interface and the peak positions of Mn overlapped with those of Al. These data confirmed that the small *B* type particles

were manganese aluminide and the Ti6Al4V and AM60B matrix interface was the preferred sites for the manganese aluminide compound to form. This conclusion was further confirmed by EDS area mapping around the Ti6Al4V particle, as shown in Fig. 4. The enrichment of Al and Mn of in the small particles and along the matrix/particle interface was clearly observed.

Fig. 5 and Fig. 6 are line and area EDS spectra around a Ti6Al4V particle in the Ti6Al4V/Mg composite after HIP. The distribution of Mg, Ti, V, Al, and Mn showed similar tendency as in the samples before HIP.

The SEM images of raw Ti6Al4V particles and the Ti6Al4V particles extracted from the samples after HIP process are illustrated in Fig. 7 and Fig. 8, respectively. The raw Ti6Al4V powders had a clean surface. In contrast, the extracted Ti6Al4V particles had various amounts of small white particles attached to the surfaces. The attached particles were usually 1-2 μm in size. The composition of the raw Ti6Al4V powders measured by EDS analysis was 91.5wt%Ti-3.5wt.%Al-5wt%V. The variation of the Al content from 6wt.% may be associated with the inaccuracy in particle surface analysis. The typical composition of the Ti6Al4V surface area free of the fine white particles was 77.3wt%Ti-9.6wt.%Al-3.3wt.%V-1.1wt.%Mn-8.7wt.%O. The typical composition of the fine white particles was 1.6wt%Ti-41.7wt.%Al-43.1wt.%Mn-13.6wt.%O. The presence of O most likely resulted from oxidation occurring during the extraction process. These results indicate the extracted particles were mainly Ti6Al4Vand a type of manganese aluminide

intermetallic compound with an Al and Mn atomic ratio approximately of 2:1, along with some oxides.

The X-Ray diffraction pattern for the extracted particles is shown in Fig. 9. The XRD spectrum reveals that the extracted particles were mainly Ti6Al4V alloy [9], Mn_5Al_8 intermetallic compound [10], and Al_2O_3 [11]. Based on the Mg-Al-Mn ternary phase diagram [12], Mn_5Al_8 intermetallic compound coexists with molten Mg-Al-Mn alloy during the melting and solidification process. Therefore, Mn_5Al_8 intermetallic compound is expected to form in the liquid Mg-Al-Mn alloy during melting. Al_2O_3 in the extracted residues was most likely formed during the particle extraction in acetic acid solution rather than formed in the alloy during melting, as the melting was conducted in Ar gas atmosphere. Compared to the Ti6Al4V/AM60B interface, Ti/Mg interface reported in reference 4 exhibits different features, where neither interfacial reaction nor mutual dissolution between Ti and Mg is observed.

3.2. Tensile tests

The results of room temperature tensile tests for AM60B, and the Ti6Al4V/AM60B composites with different Ti6Al4V concentrations are shown in Fig. 10. The addition of Ti6Al4V had no effect on either the yield strength or ultimate tensile strength of AM60B, however, the elongation was decreased by about 30%. Since Ti6Al4V has a much higher ultimate tensile strength (900 MPa [5]) than AM60B (225 MPa [8]), the observed results may be ascribed to the interfacial segregation of Mn_5Al_8. In composite materials, the mechanical properties depend strongly on the bonding between the reinforcement and the

matrix. The formation of a brittle layer at the reinforcement/matrix interface may weaken the interface and thus reduce the mechanical properties of the composite material [13]. In order to study this hypothesis, the fracture surfaces of both AM60B and Ti6Al4V/AM60B composite were examined.

Fig. 11 shows secondary electron (SE) and back-scattered electron (BSE) SEM fracture surface images of both AM60B alloy and Ti6Al4V/AM60B composite with 5% of Ti6Al4V in volume. The SE image reveals that the fracture surface of AM60B was relatively flat indicating the relatively low plastic deformation of AM60B alloy before fracture, resulting from its HCP crystal structure. The BSE image shows homogeneous distribution of the fine *B* type Mn_5Al_8 particles. The fracture surface of Ti6Al4V/AM60B composite appeared to be more torturous, possibly caused by the addition of Ti6Al4V particles which changed the microcrack propagation path. The BSE image of the fracture surface of Ti6Al4V/AM60B composite illustrates large Ti6Al4V particles, with the fine Mn_5Al_8 particles attached on their surfaces. Because the fractional area of the Ti6Al4V particles on the fracture surface was greater than the volume percentage of the particles added, it can be deduced that the Ti6Al4V/matrix interfaces are the preferred paths for crack growth, as shown with the white arrows in Fig. 11d. Furthermore, the attachment of the white Mn_5Al_8 particles to the surfaces of Ti6Al4V particles indicated that no fracture of Ti6Al4V particles had occurred. In order to further examine the crack initiation and propagation paths, the fractured tensile sample of the Ti6Al4V/AM60B composite with 5% of Ti6Al4V in volume was sectioned along the direction of the applied tensile stress. The microstructure adjacent to the fracture surface was examined by SEM. It was

observed that voids were preferentially formed at the Ti6Al4V/AM60B interface, indicating weak bonding between the matrix and Ti6Al4V particles, as illustrated by the white arrows in Figure 12a. Fig. 12b shows that the cracks went through the Ti6Al4V/matrix interface on the fracture surface. These observations confirmed that the Ti6Al4V/matrix interfaces are the preferential paths for crack growth.

From the above observations, it can be concluded that the interface of Ti6Al4V/matrix in the Ti6Al4V reinforced magnesium AM60B composite was relatively weak and failed prematurely during the tensile test. Although reinforcing a metal matrix with hard particles normally leads to lower ductility as a result of increased deformation resistance, it is believed that the weakened Ti6Al4V/matrix interfaces accounted for the degradation of ductility of the Ti6Al4V/AM60B composites. Increased addition of Ti6Al4V particles to the matrix results in more Ti6Al4V/Mg interfaces, and hence more preferred void formation sites in the Ti6Al4V/Mg composite that may in turn lead to greater degradation in the material's tensile mechanical properties. The reduction in tensile mechanical properties of a composite material caused by incorporation of a reinforcing material is observed in other magnesium matrix composites as well, including AlN/AZ91 [14] and SiC/QE22 [15]. The major reason for this phenomenon is usually undesirable reactions at the reinforcement/matrix interfaces, leading to a weak interface or depletion of some elements in the matrix that otherwise can produce other types of strengthening effect such as solution and precipitation hardening.

As is well known, the strengthening in a particulate reinforced matrix composite is a result of interactions between particles and dislocations, strain hardening, and load transfer, each of which depends on a strong interface between the particle and the matrix. So the strength of the reinforcement/matrix interface is of paramount importance in determining the overall tensile mechanical properties of the composite material. In the Ti/Mg composite reported by Hassan and Gupta [4], the Ti particles and Mg matrix demonstrates a clean and strong interface. Under a sufficiently high applied stress, the strong interface bonding makes it possible for the cracks to propagate through the matrix and the Ti particles without debonding at the Ti/matrix interface. In this case, the addition of Ti particles leads to enhanced strength of the material. In the current study, however, the Ti6Al4V/matrix interfaces were covered by a thin layer of brittle Mn_5Al_8 particles that weakened the interfaces, and thus resulted in no beneficial effect to the strength.

4. Conclusions

It is feasible to manufacture Ti6Al4V/AM60B magnesium matrix composites with homogeneous Ti6Al4V distribution and low porosity using Ar gas agitation during melting and subsequent isostatic hot pressing process. The addition of Ti6Al4V to the magnesium matrix, however, did not produce expected beneficial reinforcing effects, but only led to reduced elongation. The Ti6Al4V/matrix interfaces were found to be preferred formation sites for fine Mn_5Al_8 particles, void formation, and crack propagation paths. The formation of a brittle layer of Mn_5Al_8 at the Ti6Al4V/matrix interfaces is most likely the reason for the weakened Ti6Al4V/matrix interface.

Acknowledgement:

The authors wish to thank Moe Islam and Gord Campbell for their valuable suggestions in the course of this research work and paper manuscript preparation. The assistances by David Arnold, Bill Wells, and Mike Meinert in conducting the experiments are also gratefully acknowledged.

References:

[1]. N. Eustathopoulos, M. G. Nicholas, and B. Drevet, Wettability at high temperatures, Pregamon Materials Series, Vol. 3, Elsevier Science Ltd, UK, 1999.

[2]. S. F. Hassan, M. Gupta, Journal of Alloys and Compounds, vol. 345, no. 1-2, pp. 246-251, 28 Oct. 2002.

[3]. S. F. Hassan, K. F. Ho, and M. Gupta, Materials Letters. Vol. 58, no. 16, pp. 2143-2146. June 2004

[4]. S. F. Hassan, M. Gupta, Journal of Alloys and Compounds. Vol. 345, no. 1-2, pp. 246-251. 28 Oct. 2002.

[5]. ASM Handbook, Volume 2, Properties and Selection: Nonferrous Alloys and Special-Purpose Materials, 1990, ASM International.

[6]. Joseph I. Goldstein, Dale E. Newbury, Patrick Echlin, David C. Joy, A. D. Romig, Jr., Charles E. Lyman, Charles Fiori, and Eric Lifshin, Scanning electron microscopy and X-ray microanalysis, A text for Biologists, materials scientist, and geologists, 2nd edition, Kluwer Academic/Plenum publishers, New York, 1992.

[7]. Y. L. Liu, S. B. Kang, Materials Science and Technology Vol. 12, pp12-18. Jan. 1996.

[8]. Magnesium and Magnesium alloys, ASM specialty handbook, ASM International, Edited by Michael M. Avedesian and Hugh Baker, 1999.

[9]. JCPDS XRD diffraction card 44-1294, 1997.

[10]. JCPDS XRD diffraction card 32-0021, 1997.

[11]. JCPDS XRD diffraction card 08-0013

[12]. ASM Handbook, Volume 3, Alloy Phase Diagrams, 1990, ASM International.

[13]. D. J. Lloyd, H. P. Lagace, and A. D. Mcleod, Interfacial phenomena in metal matrix composites, Controlled Interphases in Composite Materials; Cleveland, Ohio; USA; 21-24 May 1990. pp. 359-376. 1990.

[14]. J. Schroder, K. U. Kainer, B. L. Mordike, Developments in the Science and Technology of Composite Materials. ECCM 3, Bordeaux, France, 20-23 Mar. 1989.

[15]. M. Pahutova, V. Sklenicka, K. Kucharova, and M. Svoboda, Int. J. of Materials & Product Technology, Vol. 18, Nos 1/2/3, 2003, pp 116.

Table 1. The composition of AM60B alloy.

Element	Al	Mn	Zn	Si	Cu	Fe	Ni	Mg
Content (wt.%)	5.6-6.4	0.26-0.5	<0.2	<0.05	<0.008	<0.004	<0.001	Bal.

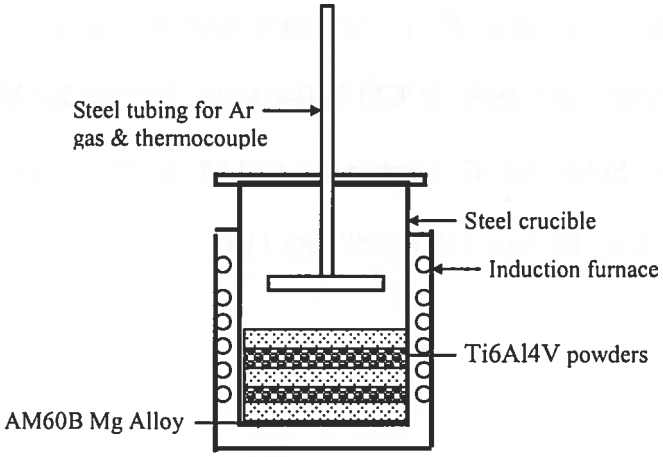

Fig. 1. Schematic illustration of melting setup.

Table 2. Phase composition (wt.%) of Ti6Al4V/AM60B composite before and after HIP.

Elements		Ti	Al	V	Mn	O	Mg
Matrix	Before HIP	Not detected	5.8	Not detected	Not detected	1.3	92.9
	After HIP	Not detected	5.9	Not detected	Not detected	2.1	92.0
Large (*A* type) particles	Before HIP	90.0	5.6	4.0	Not detected	Not detected	0.4
	After HIP	90.1	5.7	3.7	Not detected	Not detected	0.5
Small (*B* type) particles	Before HIP	Not detected	20.9	Not detected	30.9	1.3	46.9
	After HIP	Not detected	24.4	Not detected	22.7	1.4	51.2

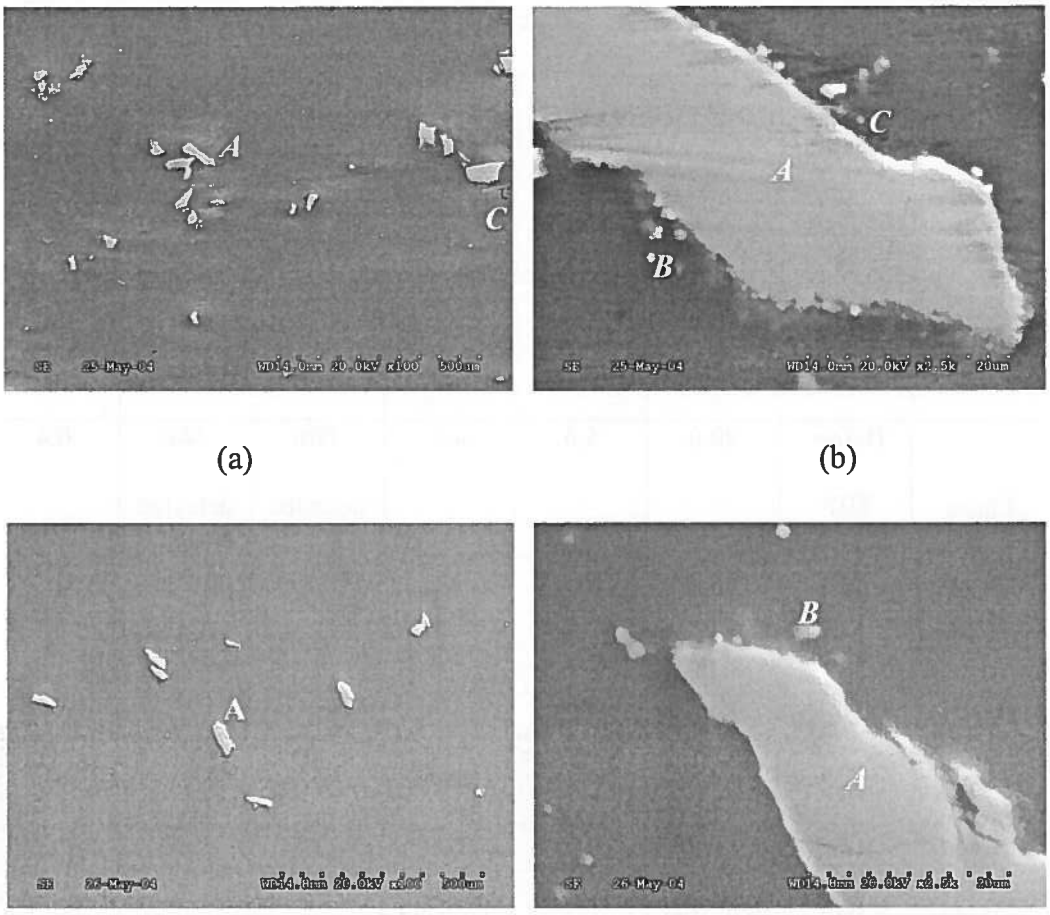

(a) (b)

(c) (d)

Fig. 2. Microstructures of 5vol.%Ti6Al4V/AM60B composite of the cross-section cut through ingot. a) Before HIP at 100X; b) Before HIP at 2500X; c) After HIP at 100X, (d) After HIP at 2500X.

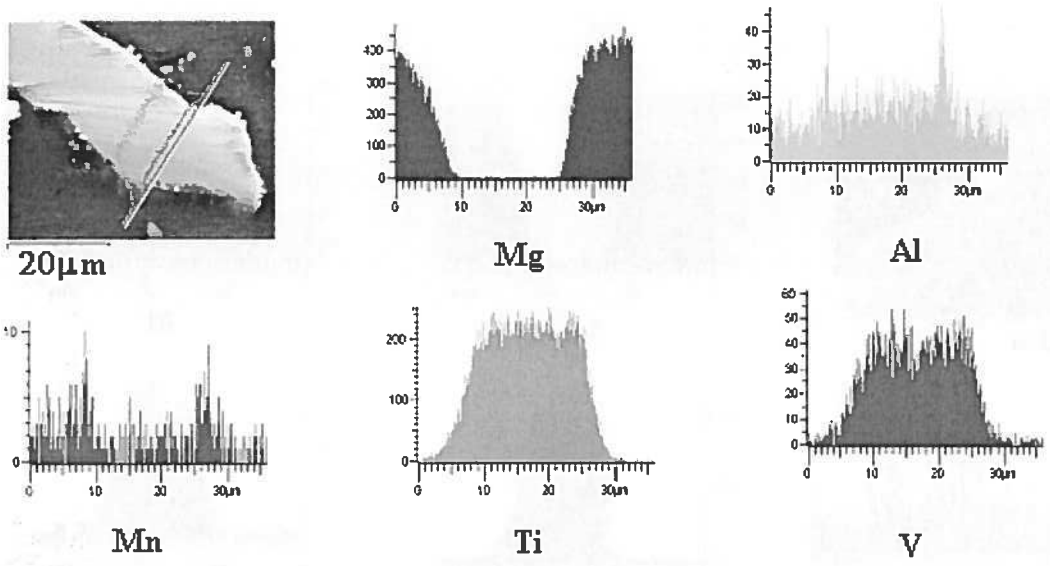

Fig. 3. EDS spectra across a Ti6Al4V particle before HIP with the composition listed in Table 2.

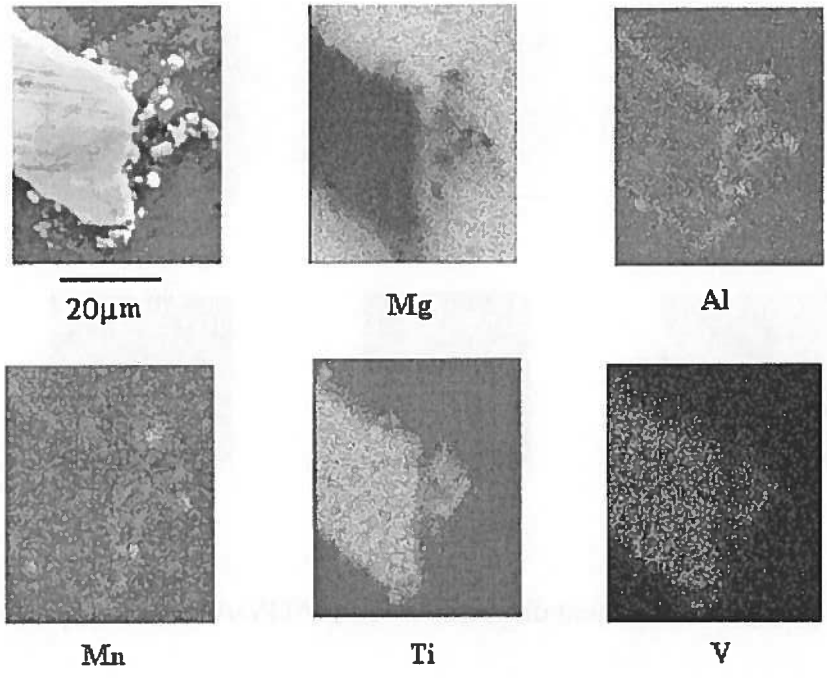

Fig. 4. Mapping of the elemental distribution around Ti6Al4V particle before HIP.

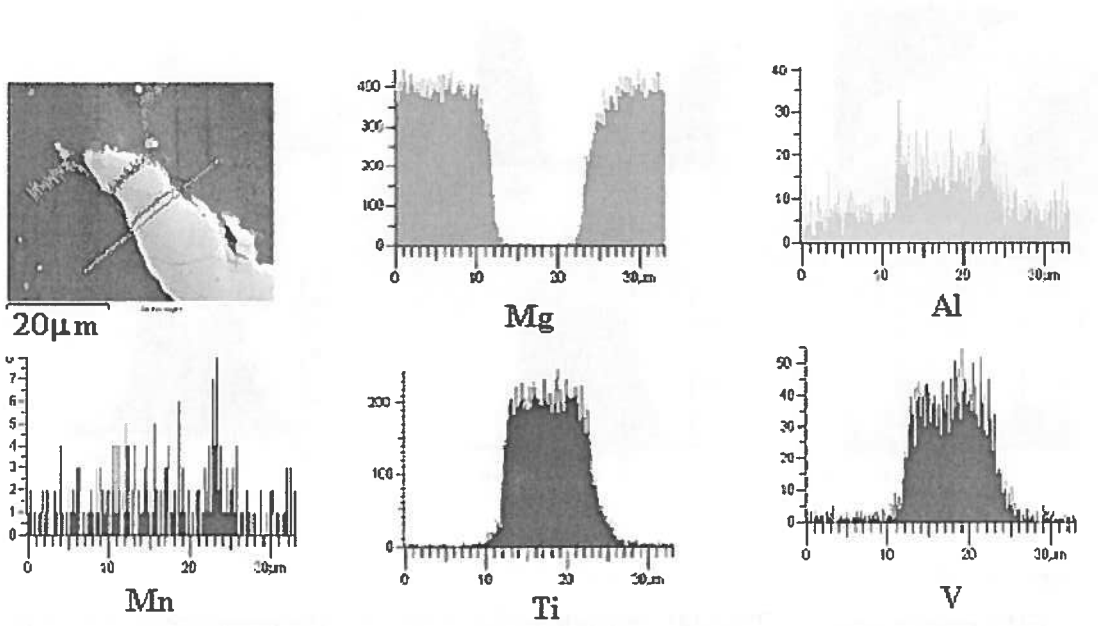

Fig. 5. EDS line analysis of the elemental distribution across Ti6Al4V after HIP with the composition listed in Table 2.

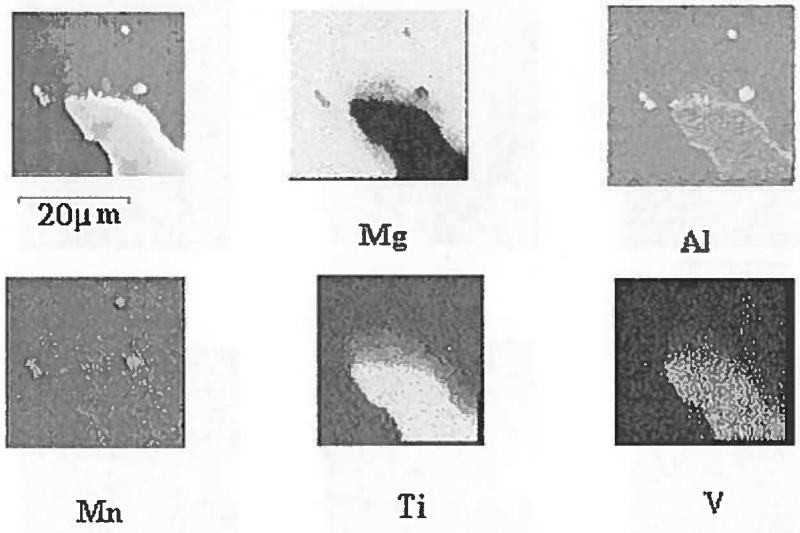

Fig. 6. The mapping of the element distribution in Ti6Al4V/AM60B composite after HIP.

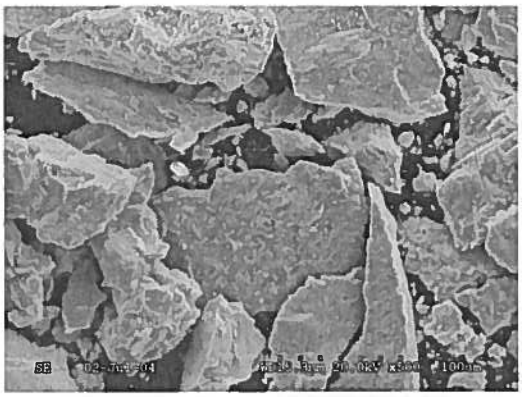

Fig. 7. The raw Ti6Al4V particles.

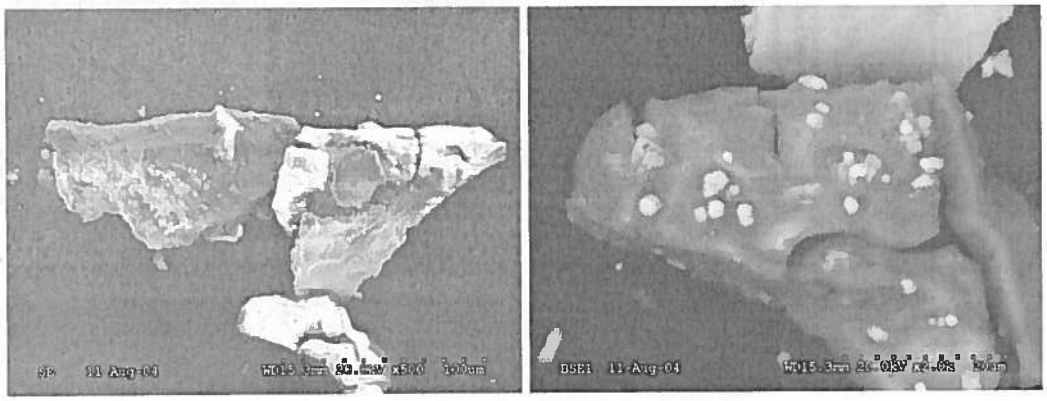

(a) (b)

Fig. 8. The extracted Ti6Al4V particles from Ti6Al4V/AM60B composite after HIP.

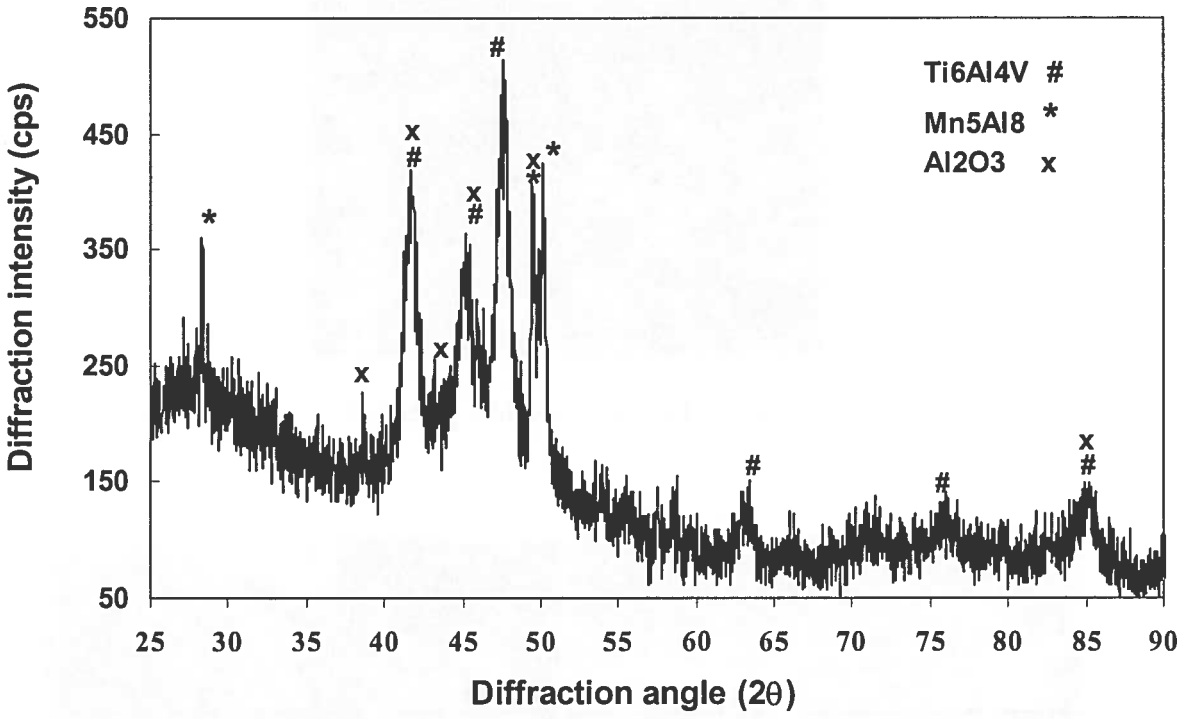

Fig. 9. The (Co-Ka) XRD analysis pattern of the extracted particles.

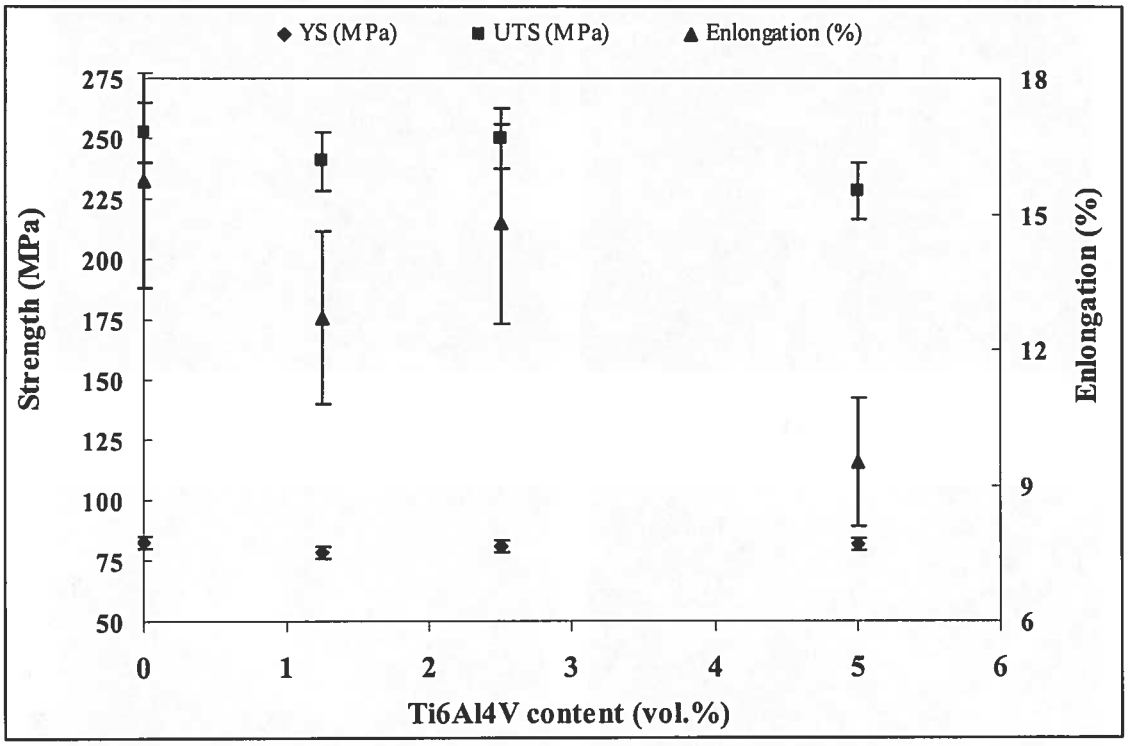

Fig. 10. The tensile properties of the Ti6Al4V/AM60B composite with different amounts of Ti6Al4V particles.

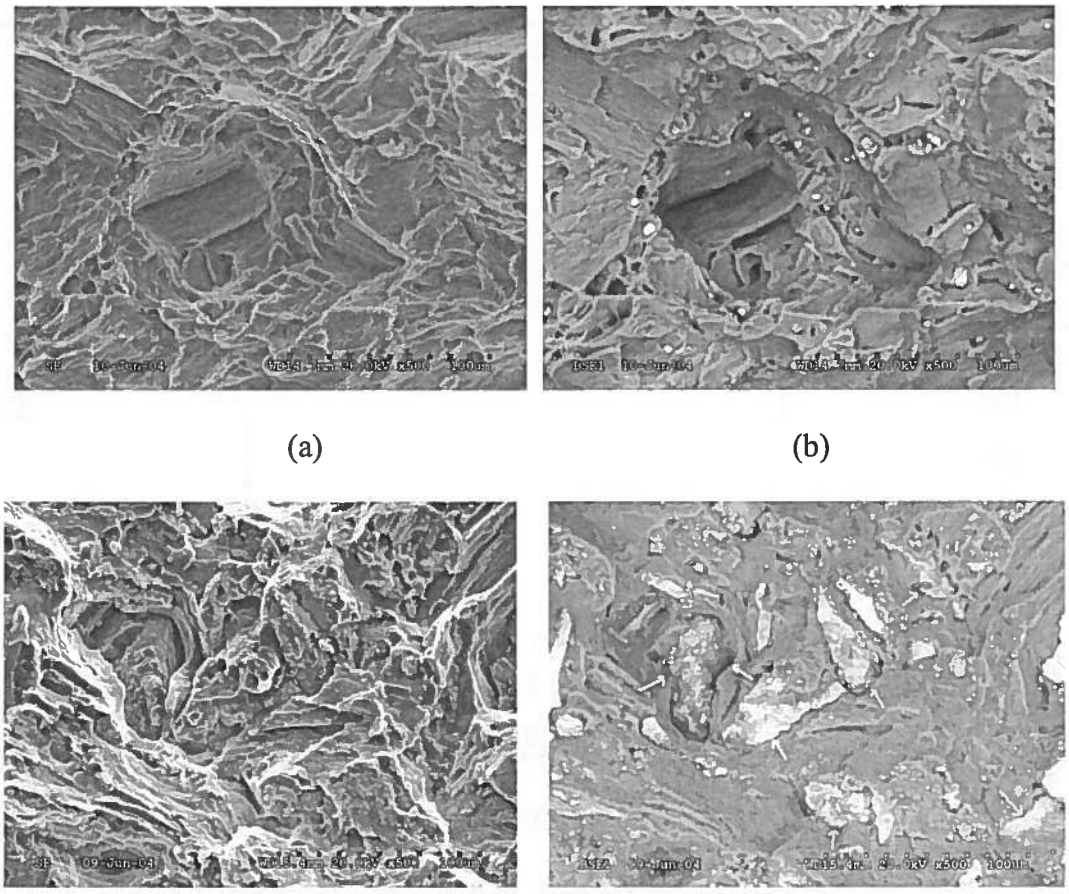

(a) (b)

(c) (d)

Fig. 11. Fracture surfaces of tensile specimens. a) SE image of AM60B; b) BSE image of AM60B, c). SE image of Ti6Al4V/AM60B with 5vol.% of Ti6Al4V, and d) BSE image of the same Ti6Al4V/AM60B composite.

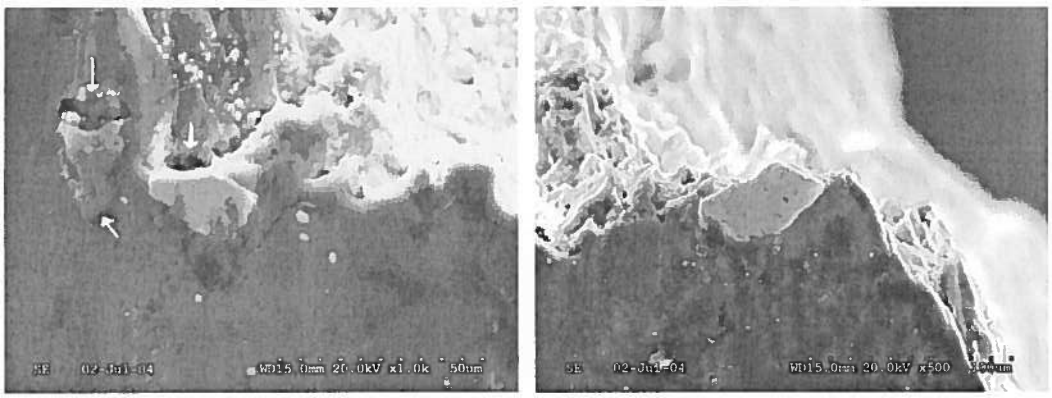

(a) (b)

Fig.12. SEM micrographs for the longitudinal cross section of the fractured tensile specimen adjacent to the fracture surface, showing cavity initiation and fracture around Ti6Al4V particles in the Ti6Al4V/AM60B composite.